Journal of Biomechanics 93 (2019) 34–41

Contents lists available at ScienceDirect

Journal of Biomechanics

journal homepage: www.elsevier.com/locate/jbiomech
www.JBiomech.com

Comparison of the hindfoot axes of a multi-segment foot model to the underlying bony anatomy

Amy B. Zavatsky [a,*], Adward M.H. Paik [a], Jessica Leitch [a], Alpesh Kothari [b,c], Julie Stebbins [c]

[a] Department of Engineering Science, University of Oxford, Oxford, UK
[b] Nuffield Department of Orthopaedics, Rheumatology and Musculoskeletal Sciences, University of Oxford, Oxford, UK
[c] Oxford Gait Laboratory, Nuffield Orthopaedic Centre, Oxford University Hospitals, Oxford, UK

ARTICLE INFO

Article history:
Accepted 5 June 2019

Keywords:
Foot
Hindfoot
Rearfoot
Calcaneus
Talus

ABSTRACT

Musculoskeletal models used in gait analysis require coordinate systems to be identified for the body segments of interest. It is not obvious how hindfoot (or rearfoot) axes defined by skin-mounted markers relate to the anatomy of the underlying bones. The aim of this study was to compare the marker-based axes of the hindfoot in a multi-segment foot model to the orientations of the talus and calcaneus as characterized by their principal axes of inertia. Twenty adult females with no known foot deformities had radio-opaque markers placed on their feet and ankles at the foot model marker locations. CT images of the feet were acquired as the participants lay supine with their feet in a semi-weight bearing posture. The spatial coordinates of the markers were obtained from the images and used to define the foot model axes. Segmented masks of the tali and calcanei were used to create 3D bone models, from which the principal axes of the bones were obtained. The orientations of the principal axes were either within the range of typical values reported in the imaging literature or differed in ways that could be explained by variations in how the angles were defined. The model hindfoot axis orientations relative to the principal axes of the bones had little bias but were highly variable. Consideration of coronal plane hindfoot alignment as measured clinically and radiographically suggested that the model hindfoot coordinate system represents the posterior calcaneal tuberosity, rather than the calcaneus as a whole.

1. Introduction

Musculoskeletal models used in gait analysis require coordinate systems to be identified for the body segments of interest. These are necessary for tracking segment motion, calculating joint angles, and defining muscle attachment points. Bone-embedded axis systems are typically specified based on palpated anatomical landmarks or other identifiable features and are assumed to represent the underlying bony anatomy.

In most multi-segment foot models, skin-mounted markers on the calcaneus are used to define the medio-lateral, antero-posterior, and proximal-distal axes of the hindfoot (or rearfoot) segment and, with tibia- and fibula-based axes, to calculate the overall motion of the ankle joint complex – a combination of the relative movements of the tibia, talus, and calcaneus. Given that the talus is inaccessible and the calcaneus has an uneven coverage of soft tissue and few easily identifiable surface landmarks, it is not obvious how the hindfoot axes defined by skin-mounted markers relate to the anatomy of these two bones.

Previous studies of gait analysis markers on the foot have not addressed this issue. Often reported are the repeatability and reproducibility of joint angles when various assessors attach markers or when foot motion is measured at multiple times and on different days (Deschamps et al., 2011, Table 5). Foot and ankle joint angles measured using skin- and bone-mounted markers have been compared (Nester et al., 2007; Westblad et al., 2002), and the skin motion artifacts of a number of gait markers on the foot and ankle have been quantified (Birch and Deschamps, 2011; Maslen and Ackland, 1994; Shultz et al., 2011; Tranberg and Karlsson, 1998). Only Brown et al. (2009) considered how foot model segment axes depend on the precision of digitized landmarks (marker points), but they did not relate their findings to the shapes of the bones themselves, only to points on the digitized bones. Furthermore, the calcaneus coordinate system used by them was constructed from four points on the lower leg and only one point on the calcaneus. Hence their study did not answer the

* Corresponding author at: Department of Engineering Science, University of Oxford, Parks Road, Oxford OX1 3PJ, UK.
E-mail address: amy.zavatsky@eng.ox.ac.uk (A.B. Zavatsky).

https://doi.org/10.1016/j.jbiomech.2019.06.006
0021-9290/

question of how the segment coordinate systems relate to the bony anatomy. Thus, the aim of the present study was to compare the marker-based axes of the hindfoot in a multi-segment foot model to the orientations of the talus and calcaneus as characterized by their principal axes of inertia.

2. Methods

Twenty adult females (age 26 ± 6 yrs, height 1.68 ± 0.07 m, weight 57.0 ± 7.0 kg) with no known foot deformities participated in the study, which was approved by the National Health Service (England) Research Ethics Committee. Radio-opaque markers (Type 2223 monitoring electrodes, 3M Healthcare, Neuss, Germany) were placed on the participants' feet and ankles at the marker locations specified for a multi-segment foot model used widely in clinical gait analysis (Stebbins et al., 2006) by a senior staff member who routinely participated in an audit of inter-rater reliability as part of the annual accreditation process of our gait laboratory. CT images (GE 64-slice Light-speed VCT scanner, 100 kV, 110 mA) were acquired as the participants lay supine with their feet in a semi-weight bearing posture, achieved using a custom-built rig (based on Wolf et al., 2007) that applied 40% bodyweight to each foot. Standard bone and soft tissue scan algorithms (slice thickness and distance both 0.625 mm) were used to scan each foot separately.

The spatial coordinates of the markers ($+x$ medial for right foot, $+y$ posterior, $+z$ proximal) were obtained from the CT images using Mimics software (version 12.11, Materialise, Leuven, Belgium). The coordinates were used to define unit vectors in the directions of the anteroposterior ($\hat{e}_{AP}$), mediolateral ($\hat{e}_{ML}$), and proximodistal ($\hat{e}_{PD}$) axes of the hindfoot segment of the foot model (Fig. 1). The long-axis of the foot ($\hat{e}_{HT}$) was taken to lie along a line connecting a marker on the posterior distal end of the calcaneus (labelled 'HEE') to one on the dorsum of the foot between the heads of the second and third metatarsals (denoted 'TOE'). To assess the inter-observer variability of the electrode marker-points ($n = 39$ feet), three raters following a standardized protocol identified the electrode coordinates on three separate foot images with full foot model marker sets (Stebbins et al., 2006). Intra-observer variability was evaluated using the marker coordinates found by one rater on one foot image on three separate occasions.

To characterize the orientations of the talus and calcaneus in three dimensions, local coordinate systems fixed in the bones were required. Since both bones lack clearly identifiable landmarks from which anatomical planes and axes can be defined, it was decided instead to use the principal axes of inertia of the bones derived from the CT scans. Segmented masks of the tali and calcanei were created using a thresholding algorithm supplemented with manual editing and exported in STL format. Each surface mask was composed, on average, of just over 11,000 triangles. SolidWorks (Dassault Systèmes SolidWorks Corp., Concord, Massachusetts, USA) was used to create 3D bone models. The unit vectors of the principal axes ($\hat{e}_i$; $i = 1, 2, 3$) of each bone (t – talus, c – calcaneus) were obtained using the mass properties tool and assuming constant density (also done by Ledoux et al., 2006).

To compare the bony alignment of the feet in the present study to previous work, nine angles between various unit vectors projected into the three standard anatomical planes were calculated (Fig. 2 and Tables 1–3). These were intended to replicate as closely as possible typical angular measurements made on plane radiographs or CT scans and used clinically. To compare the model hindfoot axes to the principal axes of the calcaneus, the long axis of the foot, and the standard anatomical directions, six other angles between unit vectors projected into the anatomical planes were calculated (Table 4).

To investigate whether the alignment of the model hindfoot axes was related to the orientations of the talus and calcaneus, unbiased estimates of Pearson's correlation coefficient (Olkin and Pratt, 1958) were calculated for the angles in Tables 1–3 in relation to those in Table 4. Also found were the p-values for testing the hypothesis that there was no relationship between the pair of angles in question. The level of significance was taken to be $\alpha = 0.05$. All angle and statistical calculations were performed in Matlab (version R2017a, The MathWorks, Inc., Natick, Massachusetts, USA).

For comparison of the model hindfoot axes and the principal axes of the bones in three dimensions, an equivalent angle-axis

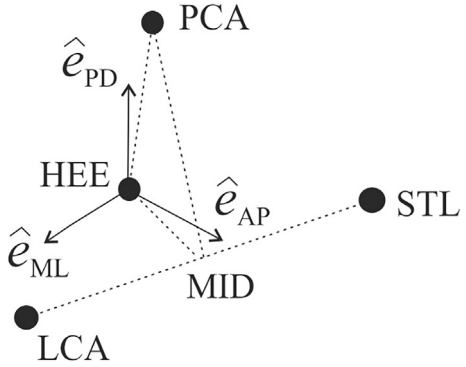

Fig. 1. The unit vectors ($\hat{e}$) in the anteroposterior (AP), mediolateral (ML), and proximal-distal (PD) directions of the hindfoot coordinate system in the Oxford multi-segment foot model (Stebbins et al., 2006), along with the gait markers used to define them (HEE = posterior distal end of calcaneus; PCA = posterior proximal end of calcaneus, STL = sustentaculum tali, LCA = lateral calcaneus; MID = midpoint of line segment connecting STL and LCA).

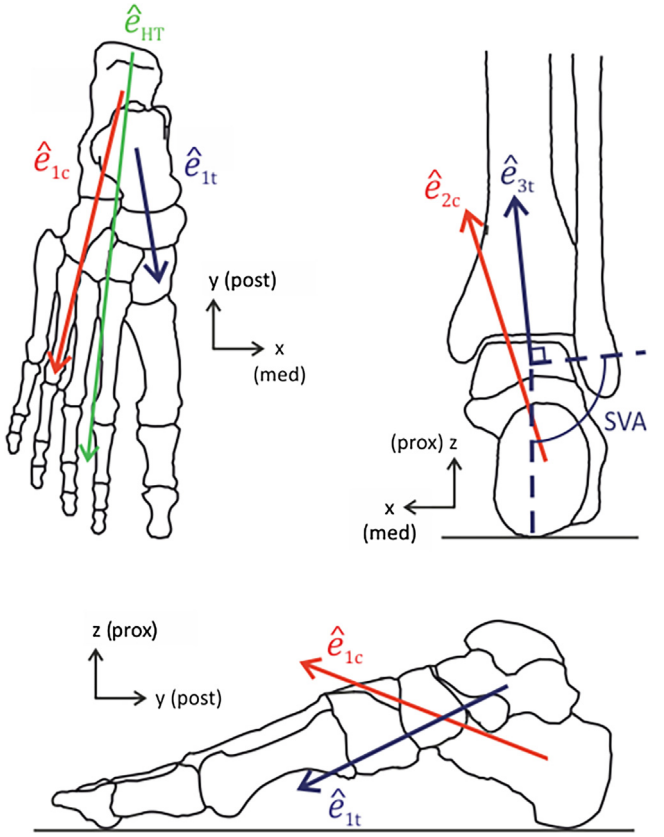

Fig. 2. Standard anatomical plane views of a right foot as defined in the CT images, with two of the principal axes of the talus ($\hat{e}_{1t}$, $\hat{e}_{3t}$) and calcaneus ($\hat{e}_{1c}$, $\hat{e}_{2c}$) and the long axis of the foot ($\hat{e}_{HT}$) shown. Top left – transverse view from above. Top right – coronal view from behind. Bottom – sagittal view from medial side.

Table 1
Typical angular measurements, calculated using the unit vectors of the first principal axes of the calcaneus and talus ($\hat{e}_{1c}$, $\hat{e}_{1t}$) and the long axis of the foot ($\hat{e}_{HT}$) projected into the transverse plane. *Angle is positive when axis points laterally compared to $\hat{e}_{HT}$. †Measurements made on CT scans. ‡Measurements made on plane radiographs (anteroposterior view).

Transverse plane x, y	Based on projections of unit vectors	Number of feet	Mean ± Std Dev	Typical values from the literature
Anteroposterior talocalcaneal angle	$\hat{e}_{1t}$,$\hat{e}_{1c}$	39	21.5° ± 5.0°	20.1° ± 2.1° (Seltzer et al., 1984)† 20.9° ± 9.2° (Richardson et al., 1992)† 21° ± 5° (Ippolito et al., 2004)† 21.1° ± 5.5° (Lamm et al., 2016)‡ 21.3°, based on (Thomas et al., 2006)‡ 23° ± 4° Ippolito et al., 2004)‡
Between calcaneus and foot long axis*	$\hat{e}_{1c}$,$\hat{e}_{HT}$	18	1.7° ± 2.8°	5.1° ± 6.3° (Thomas et al., 2006)‡
Between talus and foot long axis*	$\hat{e}_{1t}$,$\hat{e}_{HT}$	18	−17.8° ± 5.9°	−16.2° ± 7.3° (Thomas et al., 2006)‡

Table 2
Typical angular measurements, calculated using the unit vectors of the first principal axes of the calcaneus and talus ($\hat{e}_{1c}$, $\hat{e}_{1t}$) and the long axis of the foot projected into the sagittal plane ($\hat{e}_y$). All measurements from the literature were made on plane radiographs (lateral view).

Sagittal plane y, z	Based on projections of unit vectors	Number of feet	Mean ± Std Dev	Typical values from the literature
Lateral talocalcaneal angle	$\hat{e}_{1t}$, $\hat{e}_{1c}$	39	34.8° ± 4.0°	45.9° ± 7.5° (Thomas et al., 2006)
Calcaneal inclination	$\hat{e}_{1c}$, $\hat{e}_y$	40	19.6° ± 3.6°	19.6° ± 6.2° (Thomas et al., 2006) 17.9° ± 5.3° (Lamm et al., 2016)
Talar declination	$\hat{e}_{1t}$, $\hat{e}_y$	39	15.2° ± 5.0°	26.4° ± 4.1° (Thomas et al., 2006)

Table 3
Typical angular measurements, calculated using the unit vectors of the principal axes of the calcaneus and talus ($\hat{e}_{2c}$, $\hat{e}_{3t}$) projected into the coronal plane and a vertical axis ($\hat{e}_z$). *Calcaneus relative to the talus. §Angle greater than 90° indicates a valgus configuration. †Measurements made on CT scans. ‡Measurements made on plane radiographs (multiple types of frontal view).

Coronal plane x, z	Based on projections of unit vectors	Number of feet	Mean ± Std Dev	Typical values from the literature
Coronal talocalcaneal angle*	$\hat{e}_{3t}$, $\hat{e}_{2c}$	39	16.9° valgus ± 9.3°	12.5° valgus ± 3.8° (Richardson et al., 1992)†
Hindfoot/rearfoot alignment angle	$\hat{e}_{2c}$, $\hat{e}_z$	40	24.6° valgus ± 7.7°	Relative to tibial long axis: 9.1° valgus ± 4.8° (Burssens et al., 2018)† 5.6° valgus ± 5.4° (Williamson et al., 2015)‡ 5.2° valgus ± 1.6° (Seltzer et al., 1984)† 1.7° valgus (Lamm et al., 2005)‡ 1.5° valgus ± 3.4° (Lamm et al., 2016)‡ 1.5° valgus ± 2.1° (Ikoma et al., 2013)‡ 0.8° valgus ± 3.2° (Burssens et al., 2018)† 6.0° varus ± 4.6° (Johnson et al., 1999)‡ Relative to vertical: 1.6° ± 3.7° to 5.4° ± 4.8° valgus (Robinson et al., 2001)‡ 2.7° varus ± 5.3° (Van Bergeyk et al., 2002)† 9.3° varus ± 5.8° (Van Bergeyk et al., 2002)†
Subtalar vertical angle§	$\perp \hat{e}_{3t}$, $\hat{e}_z$	39	97.8° ± 6.3° (range 83°–109°)	94.6° ± 10.5°, based on (Van Bergeyk et al., 2002)† 96.1° ± 5.7° (Burssens et al., 2018)† 97.8°, based on (Colin et al., 2014†) 98°, range 85°–114° (Krähenbühl et al., 2016)†

representation was used (see, for example, Craig, 1986). The model hindfoot coordinate system was defined as ($\hat{e}_{AP}$, $\hat{e}_{ML}$, $\hat{e}_{PD}$). So that the general anatomical directions of the hindfoot and bone axes would be consistent, the calcaneus coordinate system was defined as ($\hat{e}_{1c}$, $\hat{e}_{3c}$, $\hat{e}_{2c}$) and that of the talus as ($\hat{e}_{1t}$, $\hat{e}_{2t}$, $\hat{e}_{3t}$), with unit vector directions corrected as necessary to ensure right-handed Cartesian axis systems.

3. Results

There was good inter- and intra-observer repeatability for identifying the radio-opaque marker coordinates compared to the resolution of the CT scans, with an inter-observer within-observation standard deviation of 0.40 mm and an intra-observer within-observation standard deviation of 0.18 mm. Displacement of at least one marker, usually on the heel, in the CT foot-loading rig meant that the foot model hindfoot axes could not be calculated for some feet.

The first principal axis was always directed along the long axes of the bones (anteroposteriorly). The angle between the first principal axis of the calcaneus and talus was 141.0° ± 2.8° (range 137.1°–146.6°). For the calcaneus (Fig. 3), the second and third principal axes pointed approximately in the inferior-superior and mediolateral directions, respectively; the opposite was true for the talus (Fig. 4).

Table 4
Angles between foot model hindfoot axes ($\hat{e}_{AP}$, $\hat{e}_{PD}$) and calcaneus principal axes ($\hat{e}_{1c}$, $\hat{e}_{2c}$) or reference axes ($\hat{e}_{HT}$, $\hat{e}_y$, $\hat{e}_z$), projected into the three standard anatomical planes. Sign convention: transverse plane, angle is positive when axis points laterally compared to the reference axis ($\hat{e}_{1c}$ or $\hat{e}_{HT}$); sagittal plane, angle is positive when axis points proximally compared to the reference axis ($\hat{e}_y$ or $\hat{e}_{1c}$); coronal plane, angle is positive when axis points laterally (varus) compared to the reference axis ($\hat{e}_z$ or $\hat{e}_{2c}$), with all axes positive in the proximal direction.

Plane	Angle (°)	Based on projections of unit vectors	Number of feet	Mean ± Std Dev	Range
Transverse	Between hindfoot anteroposterior axis and foot long axis	$\hat{e}_{AP}$, $\hat{e}_{HT}$	18	2.5° ± 11.9°	(−29.6°, 23.1°)
x, *y*	Between hindfoot anteroposterior axis and calcaneus long axis	$\hat{e}_{AP}$, $\hat{e}_{1c}$	18	0.9° ± 12.2°	(−30.2°, 23.2°)
Sagittal	Between hindfoot anteroposterior axis and a horizontal axis	$\hat{e}_{AP}$, $\hat{e}_y$	18	0° by definition	–
y, *z*	Between hindfoot anteroposterior axis and calcaneus long axis	$\hat{e}_{AP}$, $\hat{e}_{1c}$	18	−20.1° ± 3.4°	(−25.5°, −11.8°)
Coronal	Between hindfoot proximodistal axis and a vertical axis	$\hat{e}_{PD}$, $\hat{e}_z$	18	−4.0° ± 10.8°	(−35.7°, 8.6°)
x, *z*	Between proximo-distal axes of hindfoot and calcaneus	$\hat{e}_{PD}$, $\hat{e}_{2c}$	18	19.2° ± 9.8°	(0.2°, 34.1°)

The alignments of the principal axes of the talus and calcaneus relative to each other and to the standard anatomical directions were either within the range of typical values reported in the imaging literature (Tables 1–3) or differed in ways that could be explained by the slight variations in how the angles were defined. The only exception to this was the hindfoot (or rearfoot) alignment angle (Table 3).

In the transverse plane, the angles between the model hindfoot anteroposterior axis and the calcaneal and foot long axes had little bias, but high variability (Table 4). In the sagittal plane, the model hindfoot anteroposterior axis was by definition parallel to the plantar plane and was always rotated downwards relative to the calcaneal long axis (Table 4). In the coronal plane and similar to the transverse plane, there was high variability in the angles (Table 4). The model hindfoot proximodistal axis aligned more closely to a vertical anatomical axis than to the most proximally pointing principal axis of the calcaneus. There were significant correlations between seven of the 54 pairs of angles (Table 5), six of them involving the talus. There were no significant correlations between the model hindfoot axes and the planar talocalcaneal angles.

In three dimensions, the model hindfoot axis system was rotated on average by nearly 30° relative to the principal axis systems of both the calcaneus and the talus (Table 6). The directions of the equivalent axes of rotation implied that the model hindfoot axis system was inverted and rotated downwards and slightly

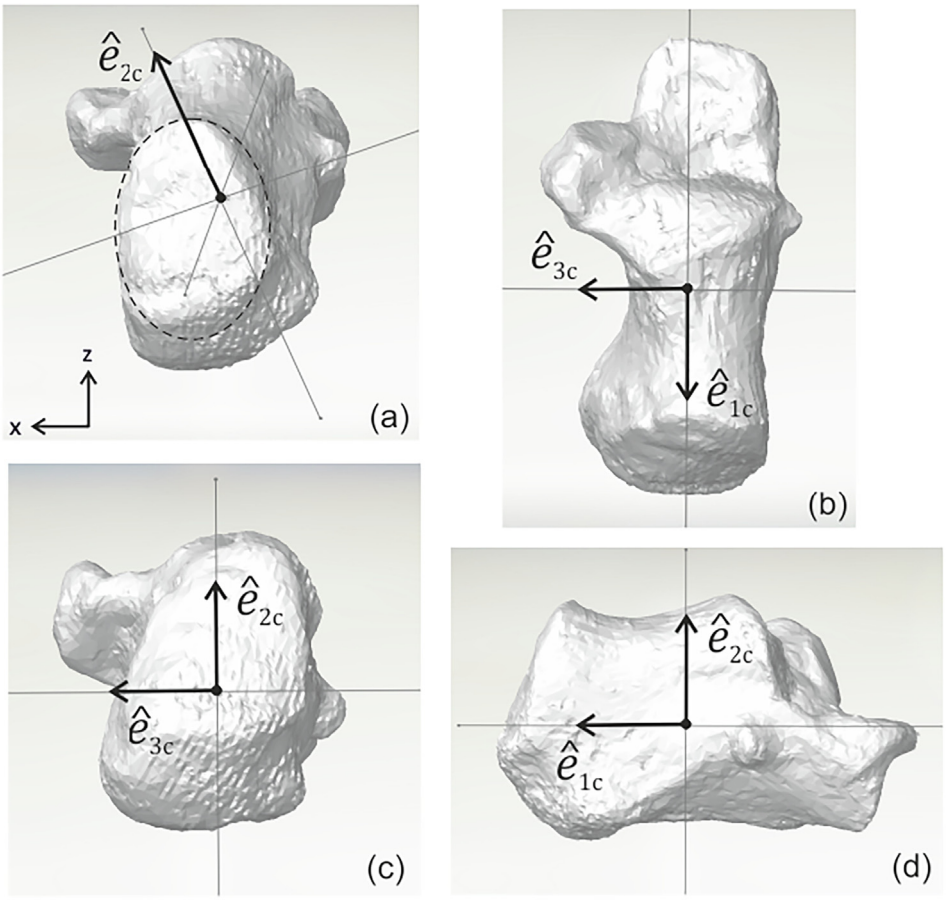

Fig. 3. Example of the calcaneus of a right foot, with principal axes $\hat{e}_{1c}$, $\hat{e}_{2c}$, and $\hat{e}_{3c}$ positioned at the centre of mass. (a) Coronal view. Dashed lines show the posterior calcaneal tuberosity. (b) View along second principal axis from above. (c) View along first principal axis from behind. (d) View along third principal axis from the lateral side.

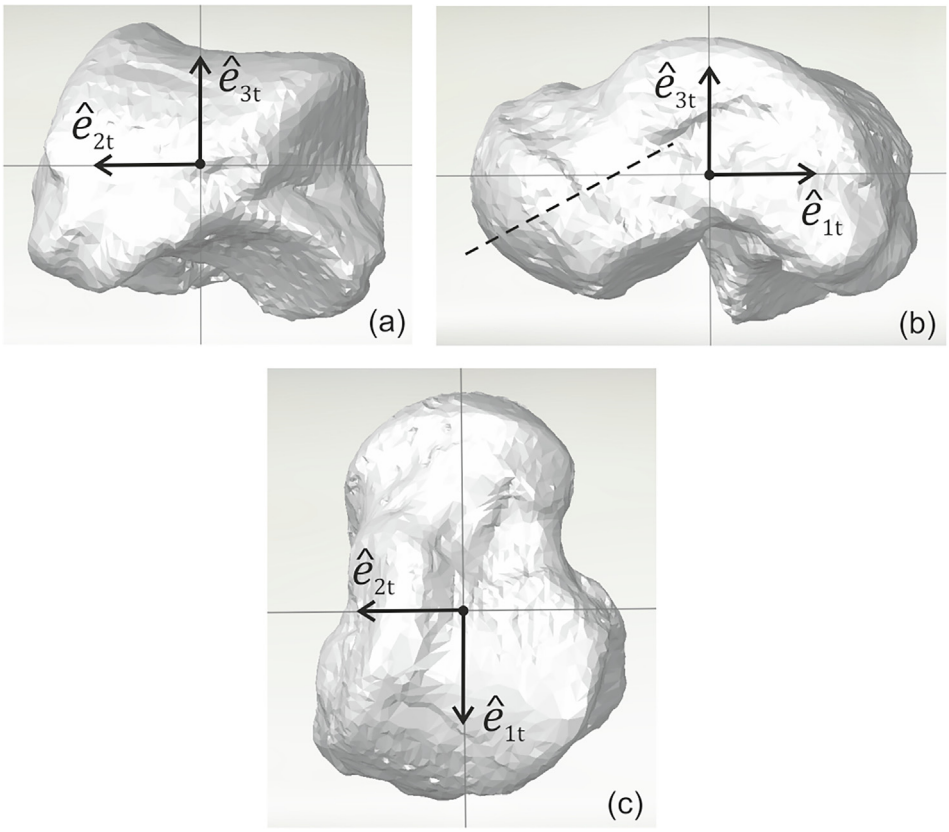

Fig. 4. Example of the talus of a right foot, with principal axes $\hat{e}_{1t}$, $\hat{e}_{2t}$, and $\hat{e}_{3t}$ positioned at the centre of mass. (a) View along first principal axis from behind. (b) View along second principal axis from the medial side. Dashed line shows the tilt of the talar neck. (c) View along third principal axis from above.

internally relative to the calcaneus principal axes. It was slightly inverted and rotated upwards and externally relative to the talus principal axes.

4. Discussion

This study compared the marker-based axes of the hindfoot in a multi-segment foot model (Stebbins et al., 2006) to the orientations of the talus and calcaneus. Even for the normal, healthy feet considered here, the model axis orientations were found to be highly variable in relation to the underlying bony anatomy and to diverge from the bone axes in three dimensions (Table 6) and in two of the six planar projection angles considered (Table 4). One of these angular differences (sagittal plane) was easily explainable, but the other (coronal plane) required more thorough investigation.

4.1. Principal axes of the bones – comparison to previous work

The agreement between the alignments of the principal axes of the talus and calcaneus relative to each other and to the standard anatomical directions (Tables 1–3) suggests that, in general, the feet included in the study were normal and that their positions in the CT scanner were close to the ones they adopted in a standing posture.

The approximate orientations of the principal axes of the bones in the anteroposterior, superior-inferior, and medio-lateral directions agreed with the results of Stindel et al. (1999a, Table 8), who studied magnetic resonance images rather than CT scans. The angle between the major (first) principal axes of the calcaneus and talus found in a related study by the same group (Stindel et al., 1999b) was very close to that of the present work (144.5° ± 2.5° compared to our 141.0° ± 2.8°).

In the transverse plane – or anteroposterior (AP) radiography view (Table 1), the talocalcaneal angle was in good agreement with several other studies. The close and consistent alignment of the calcaneal axis with the long axis of the foot was not surprising, since it is generally agreed that the long axis of the calcaneus normally extends along the line of the 4th metatarsal (Coughlin et al., 2013). That the long axis of the talus pointed medially to the long axis of the foot was consistent with description of the talar axis normally extending along the first metatarsal (Coughlin et al., 2013).

In the sagittal plane – or lateral radiography view (Table 2), the calcaneal inclination agreed closely with Thomas et al. (2006), whilst the talar declination was around 10° lower than what they reported. This mismatch in declination can be explained by the difference in how the talus axis was defined: using the talar neck only (Thomas et al., 2006) versus representing the entire talar body by the first principal axis. Taking into account the entire body would likely lead to a more shallow declination (Fig. 4b and the images of the talus in Bonnel et al. (2011) illustrate this clearly.). The lateral talocalcaneal angle being lower than that of Thomas et al. (2006) is consistent with this explanation.

In the coronal plane – or frontal radiography view (Table 3), the talocalcaneal angle was in reasonable agreement with the literature. The subtalar vertical angle, derived from the most vertical principal axis of the talus, was in very good agreement with previous work, despite a difference in how the angle was defined. On CT scans, the angle was measured relative to vertical using a line across the posterior facet of the subtalar joint. All studies, including the present one, found a slight valgus orientation of the (distal) talus on average.

Table 5
Unbiased estimates of Pearson's correlation coefficient (Olkin and Pratt, 1958) and the associated levels of significance for combinations of angles in Tables 1–3 and 4. Significant correlations ($p < 0.05$) are shown in bold font.

		Plane	Transverse x, y			Sagittal y, z			Coronal x, z		
	Angle (°)		Anteroposterior talocalcaneal angle	Between calcaneus and foot long axis	Between talus and foot long axis	Lateral talocalcaneal angle	Calcaneal inclination	Talar declination	Coronal talocalcaneal angle	Hindfoot alignment angle (with tibia)	Subtalar vertical angle
Plane	Angle (°)	Based on projections of unit vectors	$\hat{e}_{1t}$, $\hat{e}_{1c}$	$\hat{e}_{1c}$, $\hat{e}_{HT}$	$\hat{e}_{1t}$, $\hat{e}_{HT}$	$\hat{e}_{1t}$, $\hat{e}_{1c}$	$\hat{e}_{1c}$, $\hat{e}_y$	$\hat{e}_{1t}$, $\hat{e}_y$	$\hat{e}_{3t}$, $\hat{e}_{2c}$	$\hat{e}_{2c}$, $\hat{e}_z$	$\perp \hat{e}_{3t}$, $\hat{e}_z$
Transverse x, y	Between hindfoot anteroposterior axis and foot long axis	$\hat{e}_{AP}$, $\hat{e}_{HT}$	0.4612 $p = 0.0704$	0.0030 $p = 0.9908$	−0.4037 $p = 0.1190$	−0.2629 $p = 0.3233$	−0.1291 $p = 0.6206$	−0.0873 $p = 0.7471$	0.0392 $p = 0.8850$	0.4549 $p = 0.0651$	**−0.5559** **$p = 0.0242$**
	Between hindfoot anteroposterior axis and calcaneus long axis	$\hat{e}_{AP}$, $\hat{e}_{1c}$	0.4419 $p = 0.0847$	−0.2348 $p = 0.3628$	**−0.5037** **$p = 0.0452$**	−0.1346 $p = 0.6181$	−0.1983 $p = 0.4441$	0.0865 $p = 0.7493$	0.1625 $p = 0.5463$	0.3533 $p = 0.1623$	**−0.5812** **$p = 0.0173$**
Sagittal y, z	Between hindfoot anteroposterior axis and a horizontal axis	$\hat{e}_{AP}$, $\hat{e}_y$	–	–	–	–	–	–	–	–	–
	Between hindfoot anteroposterior axis and calcaneus long axis	$\hat{e}_{AP}$, $\hat{e}_{1c}$	0.4939 $p = 0.0503$	−0.3145 $p = 0.2171$	**−0.5928** **$p = 0.0147$**	−0.3527 $p = 0.1782$	−1 n/a	**0.6186** **$p = 0.0100$**	0.2766 $p = 0.2977$	−0.1629 $p = 0.5309$	−0.1565 $p = 0.5615$
Coronal x, z	Between hindfoot proximodistal axis and a vertical axis	$\hat{e}_{PD}$, $\hat{e}_z$	0.4374 $p = 0.0884$	−0.0179 $p = 0.9454$	−0.3915 $p = 0.1317$	0.0316 $p = 0.9074$	−0.0206 $p = 0.9374$	0.0670 $p = 0.8046$	−0.0721 $p = 0.7902$	**0.5151** **$p = 0.0332$**	**−0.4963** **$p = 0.0490$**
	Between proximo-distal axes of hindfoot and calcaneus	$\hat{e}_{PD}$, $\hat{e}_{2c}$	−0.0029 $p = 0.9914$	−0.3494 $p = 0.1675$	−0.1672 $p = 0.5345$	0.3003 $p = 0.2565$	−0.1596 $p = 0.5394$	0.4148 $p = 0.1082$	0.4828 $p = 0.0566$	−0.2886 $p = 0.2595$	−0.2144 $p = 0.4235$

It was in the hindfoot alignment in the coronal plane (Table 3) where the results of the present study diverged most from the literature. This was very likely because the most vertical principal axis of the calcaneus and the hindfoot axis identified radiographically in the other studies represent very different things. The principal axes (Fig. 3) relate to the distribution of bone mass over the entire bone volume, whereas the radiographic measures rely mainly on identifying the medial and lateral edges of the posterior calcaneal tuberosity (Fig. 3a) to define the hindfoot axis, although the precise definition varies from study to study (see references in Table 3).

Most previous imaging work (Table 3) agreed on there being a hindfoot valgus relative to the tibia long axis, despite variations in how the images were acquired and measured. Also, as Slullitel et al. (2017) and others have pointed out, it is difficult to measure hindfoot alignment in the coronal plane radiographically because of the superposition of the calcaneus and the rest of the foot. Procedural differences between the previous studies in Table 3 included the x-ray view used (hindfoot alignment view, long axial view, or other) or CT slice considered, the foot alignment, the amount of weight-bearing, whether the stance was relaxed or in a calcaneus-neutral position, the size of sample measured, the precise definition of the hindfoot axis, and the reliability and repeatability of the measurement itself.

4.2. Multi-segment foot model axes

Given the discussion above comparing the principal axes of the bones to previous work, it is now easier to explain the discrepancy between the calcaneal second principal axis and the model hindfoot proximo-distal axis in the coronal plane. Similar to imaging measurements of the hindfoot/rearfoot alignment angle (Table 3), the model hindfoot axis definitions (Stebbins et al., 2006) are based partly on points located on the posterior calcaneal tuberosity. These define a noticeably different vertical orientation for the hindfoot than that of the calcaneus taken as a whole (Fig. 3a). That the model hindfoot axis alignment with the vertical (Table 4) was within the range of hindfoot alignment angles measured in the imaging studies (Table 3) is therefore not unexpected. The large ranges of nearly all the angles in Table 4 can be explained by the irregular shape of the calcaneus and its variation across the population (Bruckner, 1987), the range of static weightbearing hindfoot alignments seen in adults (Waldecker et al., 2012), and the known difficulties of measuring the alignment angle reliably (Haight et al., 2005; Menz, 1995).

There were no correlations (Table 5) between the foot model angles (Table 4) and any of the talocalcaneal angles (Tables 1–3), all of which were within normal ranges. Whether this would still be true for feet with deformity cannot be judged from the present results. Six of the seven significant correlations in Table 5 relate to the talus, with half of these involving the subtalar vertical angle (as defined by $\perp \hat{e}_{3t}$, $\hat{e}_z$ in the coronal plane). In some sense, this is to be expected, since the frontal plane position of the calcaneus (represented here by the angle between $\hat{e}_{PD}$ and $\hat{e}_z$) is usually taken to be indicative of the alignment of the subtalar joint (Menz, 1995). That the alignment of $\hat{e}_{AP}$ in the transverse plane is also correlated with the subtalar joint angle (Table 5) can be explained by the fact that any rotation of the talus or the calcaneus about an axis in the anteroposterior direction (perpendicular to the coronal plane) would be expected to cause the alignment of the bone to change in both the coronal and transverse planes. This is because the long axes of these bones are unlikely both to lie in a sagittal plane.

The two correlations involving $\hat{e}_{AP}$ and $\hat{e}_{1c}$ in the sagittal plane (Table 5) must be interpreted in the knowledge that, by definition, $\hat{e}_{AP} = \hat{e}_y$. The correlation between $\hat{e}_{AP}$, $\hat{e}_{1c}$ and $\hat{e}_{1t}$, $\hat{e}_y$ in the sagittal

Table 6
The equivalent angles and axes of rotation for the model hindfoot axis system ($\hat{e}_{AP}$, $\hat{e}_{ML}$, $\hat{e}_{PD}$) compared to the principal axis systems of the calcaneus ($\hat{e}_{1c}$, $\hat{e}_{3c}$, $\hat{e}_{2c}$) and talus ($\hat{e}_{1t}$, $\hat{e}_{2t}$, $\hat{e}_{3t}$). Positive *x*, *y*, and *z* directions are, respectively, medially (for a right foot), posteriorly, and proximally, as shown in Fig. 2.

	Number of Feet	Equivalent Angle (°)		Equivalent axis components		
		Mean ± Std Dev	Range	$\hat{e}_x$	$\hat{e}_y$	$\hat{e}_z$
Hindfoot/Calcaneus	18	28.7 ± 6.0	(16.7, 40.7)	0.591 ± 0.228	−0.617 ± 0.329	0.073 ± 0.346
Hindfoot/Talus	18	28.7 ± 9.9	(18.2, 48.0)	−0.540 ± 0.168	−0.080 ± 0.339	−0.666 ± 0.364

plane implies that $\hat{e}_{1c}$ and $\hat{e}_{1t}$ are related. This makes sense, since any change in the calcaneal pitch must be accompanied by an adjustment in talar declination so that both the hindfoot and forefoot remain in contact with the ground. The correlation between $\hat{e}_{AP}$ and $\hat{e}_{1c}$ in the sagittal plane and the talar alignment in the transverse plane (defined by $\hat{e}_{1t}$, $\hat{e}_{HT}$) could relate to the need to maintain congruity in the subtalar joint.

4.3. Implications of the results

The model hindfoot coordinate system appears to represent the posterior calcaneal tuberosity, rather than the calcaneus as a whole. This is most likely because the anterior portion of the calcaneus is inaccessible and markers must be placed on the heel, where the main shape feature is the posterior tuberosity.

Imaging of the foot with the motion-tracking markers attached, as done in the present work with CT and in the foot model of Kidder et al. (1996) with plane radiographs, could be used to realign the marker-based coordinate systems with those of the bones or anatomical planes or to quantify any misalignment. Given the present results and that clinical and radiographic measures of hindfoot coronal alignment are known to differ (Lamm et al., 2005; Slullitel et al., 2017), disparities are to be expected. In a clinical situation, however, adding imaging to a gait assessment would have to be balanced against the additional time and expense involved, although it could be justified for feet with deformity. If a calcaneal osteotomy is being considered, then knowledge of the orientation of the entire bone, rather than just the coronal plane alignment of the posterior calcaneal tuberosity as indicated by the gait markers, could help to refine the surgical procedure.

Being aware of the variability of the model hindfoot coordinate system alignment with the underlying anatomy and taking practical steps to limit this is also important. Clear marker placement protocols and proper instruction in marker placement for new clinical gait practitioners are essential, and particular attention should be paid to intra- and inter-rater reliability of marker placement. Use of a calcaneal marker placement device (Deschamps et al., 2014) or heel alignment device (Simon et al., 2006) could also be of benefit. It is interesting to recall that, in defining a coordinate system for the calcaneus, Brown et al. (2009) chose to use points on the tibia and fibula, with only a single point on the heel, in order to reduce errors in axis alignment.

In multi-segment foot models, the third rotation in the Euler angle sequence for the ankle (inversion-eversion or abduction-adduction, depending on the model) takes place about an axis of the hindfoot coordinate system. The results of the present work imply that the orientation of this axis relative to the standard planes of the foot or to the bony anatomy of the calcaneus and talus is likely to be subject-specific.

4.4. Limitations

The present work has its limitations, including the relatively small cohort and the inclusion of normal adult female feet only. Ideally, a much larger sample and one more representative of the patient groups seen in clinical gait laboratories would be studied. Although participants were measured in a simulated weight-bearing position, their body position in the CT scanner was supine and their foot alignment was not fully standardized. For some participants, there was an unfortunate loss of data due to markers on the heel being displaced due to contact with the back of the foot-loading device. These drawbacks could be overcome by use of an upright weight-bearing CT scanner (as in Burssens et al., 2018; Colin et al., 2014), which might also give a more extended view of the tibial shaft so that the model hindfoot axis alignment with the tibia in the coronal plane could be measured. The relationship between the foot model axes and the bone axes was considered here only in a single static position. Of course, this could change over a gait cycle due to movement of the markers over skin and other soft tissues. Measuring multiple static foot positions, tracking the foot using bone-mounted motion capture markers during gait, or imaging the feet during walking with bi-planar x-ray fluoroscopy would give a more complete picture of how the foot model axes relate to the underlying bony anatomy. Finally, the use of a single foot model (Stebbins et al., 2006) in the present study was not seen as a limitation, since the marker locations on the hindfoot are similar to those used in other multi-segment foot models (Kidder et al., 1996; Simon et al., 2006; Leardini et al., 2007; Saraswat et al., 2012).

5. Conclusions

The foot model hindfoot axis orientations relative to the principal axes of the talus and calcaneus had little bias but were highly variable. Consideration of coronal plane hindfoot alignment as measured clinically and radiographically suggested that the model hindfoot coordinate system represents the posterior calcaneal tuberosity, rather than the calcaneus as a whole.

Declaration of Competing Interest

The authors declare no conflicts of interest.

Acknowledgements

Jessica Leitch was funded by the Engineering and Physical Sciences Research Council (EPSRC, UK) as a part of the Life Sciences Interface Doctoral Training Centre at the University of Oxford. Alpesh Kothari was supported by a research training fellowship from the charity Action Medical Research (UK).

References

Birch, I., Deschamps, K., 2011. Quantification of skin marker movement at the malleoli and talar heads. J. Am. Podiatr. Med. Assoc. 101, 497–504.
Bonnel, F., Teissier, P., Maestro, M., Ferré, B., Toullec, E., 2011. Biometry of bone components in the talonavicular joint: a cadaver study. Orthop. Traumatol. Surg. Res. 97S, S66–S73.
Brown, K.M., Bursey, D.E., Arneson, L.J., Andrews, C.A., Ludewig, P.M., Glasoe, W.M., 2009. Consideration of digitization precision when building local coordinate axes for a foot model. J. Biomech. 42, 1263–1269.
Bruckner, J., 1987. Variations in the human subtalar joint. J. Orthop. Sports Phys. Therapy 8, 489–494.
Burssens, A., Van Herzele, E., Leenders, T., Clockaerts, S., Buedts, K., Vandeputte, G., Victor, J., 2018. Weightbearing CT in normal hindfoot alignment – presence of a constitutional valgus? J. Foot Ankle Surg. 24, 213–218.

Colin, F., Lang, T., Zwicky, L., Hintermann, B., Knupp, M., 2014. Subtalar joint configuration on weightbearing CT scan. Foot Ankle Int. 35, 1057–1062.
Coughlin, M.J., Saltzman, C.L., Mann, R.A., 2013. Mann's Surgery of the Foot and Ankle (eBook). Elsevier Health Sciences, London.
Craig, J.J., 1986. Introduction to Robotics. Addison-Wesley Publishing Co., Reading, Massachusetts.
Deschamps, K., Sates, F., Roosen, P., Nobels, F., Desloovere, K., Bruyninckx, H., Matricali, G.A., 2011. Body of evidence supporting the clinical use of 3D multisegment foot models: a systematic review. Gait Post. 33, 338–349.
Deschamps, K., Rosen, P., Birch, I., Dingenen, B., Buryninckx, H., Desloovere, K., Aertbelien, E., Staes, F., 2014. A novel device for standardizing marker placement at the calcaneus. J. Am. Podiatr. Med. Assoc. 104, 43–49.
Haight, H.J., Dahm, D.L., Smith, J., Drause, D.A., 2005. Measuring standing hindfoot alignment: reliability of goniometric and visual measurements. Arch. Phys. Med. Rehabil. 86, 571–575.
Ikoma, K., Noguchi, M., Nagasawa, K., Maki, M., Kido, M., Hara, Y., Kubo, T., 2013. A new radiographic view of the hindfoot. J. Foot Ankle Res. 6, 48.
Ippolito, E., Fraracci, L., Farsetti, P., De Maio, F., 2004. Validity of the anteroposterior talocalcaneal angle to assess congenital clubfoot correction. Am. J. Roentgenol. 182, 1279–1282.
Johnson, J.E., Lamdan, R., Granberry, W.F., Harris, G.F., Carrera, G.F., 1999. Hindfoot coronal alignment: a modified radiographic method. Foot Ankle Int. 20, 818–825.
Kidder, S.M., Abuzzahab Jr., F.S., Harris, G.F., Johnson, J.E., 1996. A system for the analysis of foot and ankle kinematics during gait. IEEE Trans. Rehabil. Eng. 4, 25–32.
Krähenbühl, N., Tschuck, M., Bolliger, L., Hintermann, B., Knupp, M., 2016. Orientation of the subtalar joint: measurement and reliability using weightbearing CT scans. Foot Ankle Int. 37, 109–114.
Lamm, B.M., Mendicino, R.W., Catanzariti, A.R., Hillstrom, H.J., 2005. Static rearfoot alignment: a comparison of clinical and radiographic measures. J. Am. Podiatr. Med. Assoc. 95, 26–33.
Lamm, B.M., Stasko, P.A., Gesheff, M.G., Bhave, A., 2016. Normal foot and ankle radiographic angles, measurements, and reference points. J. Foot Ankle Surg. 55, 991–998.
Leardini, A., Benedetti, M.G., Berti, L., Bettinelli, D., Nativo, R., Giannini, S., 2007. Rear-foot, mid-foot and fore-foot motion during the stance phase of gait. Gait Post. 25, 453–462.
Ledoux, W.R., Rohr, E.S., Ching, R.P., Sangerozan, B.J., 2006. Effect of foot shape on the three-dimensional position of foot bones. J. Orthop. Res. 24, 2176–2186.
Maslen, B.A., Ackland, T.R., 1994. Radiographic study of skin displacement errors in the foot and ankle during standing. Clin. Biomech. 9, 291–296.
Menz, H.B., 1995. Clinical hindfoot measurement: a critical review of the literature. Foot 5, 57–64.
Nester, C., Jones, R.K., Liu, A., Howard, D., Lundberg, A., Arndt, A., Lundgren, P., Stacoff, A., Wolf, P., 2007. Foot kinematics during walking measured using bone and surface mounted markers. J. Biomech. 40, 3412–3423.
Olkin, I., Pratt, J.W., 1958. Unbiased estimation of certain correlation coefficients. Ann. Math. Stat. 29, 201–211.
Richardson, M.L., Vu, M.V., Vincent, L.M., Sangeorzan, B.J., Benirschke, S.K., 1992. CT measurement of the calcaneal varus angle in the normal and fractured hindfoot. J. Comput. Assist. Tomogr. 16, 261–264.
Robinson, I., Dyson, R., Halson-Brown, S., 2001. Reliability of clinical and radiographic measurement of rearfoot alignment in a patient population. Foot 11, 2–9.
Saraswat, P., MacWilliams, B.A., Davis, R.B., 2012. A multi-segment foot model based on anatomically registered technical coordinate systems: method repeatability in pediatric feet. Gait Post. 35, 547–555.
Seltzer, S.E., Weissman, B.N., Braunstein, E.M., Adams, D.F., Thomas, W.H., 1984. Computed tomography of the hindfoot. J. Comput. Assist. Tomogr. 8, 488–497.
Shultz, R., Kedgley, A.E., Jenkyn, T.R., 2011. Quantifying skin motion artifact error of the hindfoot and forefoot marker clusters with the optical tracking of a multi-segment foot model using single-plane fluoroscopy. Gait Post. 32, 44–48.
Simon, J., Doederlein, L., McIntosh, A.S., Metaxiotis, D., Bock, H.G., Wolf, S.I., 2006. The Heidelberg foot measurement method: development, description and assessment. Gait Post. 23, 411–424.
Slullitel, G., Álvarex, V., Lopez, V., Calvi, J.P., Calvo, A.B., 2017. How accurate is clinical evaluation in hindfoot coronal alignment? Foot Ankle Orthop. 2, 1–7.
Stebbins, J., Harrington, M., Thompson, N., Zavatsky, A., Theologis, T., 2006. Repeatability of a model for measuring multi-segment foot kinematics in children. Gait Post. 23, 401–410.
Stindel, E., Udupa, J.K., Hirsch, B.E., Odhner, D., 1999a. 3D MR image analysis of the morphology of the rear foot: application to the classification of bones. Comput. Med. Imag. Graph. 23, 75–83.
Stindel, E., Udupa, J.K., Hirsch, B.E., Odhner, D., 1999b. A charaterization of the geometric architecture or the peritalar joint complex via MRI, an aid to classification of foot type. IEEE Trans. Med. Imag. 18, 753–763.
Thomas, J.L., Kunkel, M.W., Lopez, R., Sparks, D., 2006. Radiographic values of the adult foot in a standardized population. J. Foot Ankle Surg. 45, 3–12.
Tranberg, R., Karlsson, D., 1998. The relative skin movement of the foot: a 2-D roentgen photogrammetry study. Clin. Biomech. 13, 71–76.
Van Bergeyk, A., Younger, A., Carson, B., 2002. CT analysis of hindfoot alignment in chronic lateral ankle instability. Foot Ankle Int. 23, 37–42.
Waldecker, U., Hofmann, G., Drewitz, S., 2012. Epidemiologic investigation of 1394 feet: coincidence of hindfoot malalignment and Achilles tendon disorders. Foot Ankle Surg. 18, 119–123.
Westblad, P., Hashimoto, T., Winson, I., Lundberg, A., Arndt, A., 2002. Differences in ankle-joint complex motion during the stance phase of walking as measured by superficial and bone-anchored markers. Foot Ankle Int. 23, 856–863.
Williamson, E.R.C., Chan, J.Y., Burket, J.C., Deland, J.T., Ellis, S.J., 2015. New radiographic parameter assessing hindfoot alignment in stage II adult-acquired flatfoot deformity. Foot Ankle Int. 36, 417–423.
Wolf, P., Luechinger, R., Boesiger, P., Stuessi, E., Stacoff, A., 2007. A MR imaging procedure to measure tarsal bone rotations. J. Biomech. Eng. 129, 931–936.